

# Hall Thruster Plume Measurements from High-Speed Dual Langmuir Probes with Ion Saturation Reference

Michael Sekerak  
University of Michigan  
Plasmadynamics and  
Electric Propulsion  
Laboratory  
1919 Green Rd, B107  
Ann Arbor, MI 48105  
734-764-4199  
msekerak@umich.edu

Michael McDonald  
University of Michigan  
Plasmadynamics and  
Electric Propulsion  
Laboratory  
1919 Green Rd, B107  
Ann Arbor, MI 48105  
734-764-4199  
msmcdon@umich.edu

Richard Hofer  
Jet Propulsion Laboratory  
California Institute of  
Technology  
Electric Propulsion Group  
4800 Oak Grove Drive  
MS 125-109  
Pasadena, CA 91109  
818-393-2506  
richard.r.hofer@jpl.nasa.gov

Alec Gallimore  
University of Michigan  
Plasmadynamics and  
Electric Propulsion  
Laboratory  
1919 Green Rd, B107  
Ann Arbor, MI 48105  
734-764-8224  
alec.gallimore@umich.edu

**Abstract** — The plasma plume of a 6 kW Hall Effect Thruster (HET) has been investigated in order to determine time-averaged and time-resolved plasma properties in a 2-D plane. HETs are steady-state devices with a multitude of kilohertz and faster plasma oscillations that are poorly understood yet impact their performance and may interact with spacecraft subsystems. HETs are known to operate in different modes with differing efficiencies and plasma characteristics, particularly the axial breathing mode and the azimuthal spoke mode. In order to investigate these phenomena, high-speed diagnostics are needed to observe time-resolved plasma properties and correlate them to thruster operating conditions. A new technique called the High-speed Dual Langmuir Probe with Ion Saturation Reference (HDLP-ISR) builds on recent results using an active and an insulated or null probe in conjunction with a third, fixed-bias electrode maintained in ion saturation for ion density measurements. The HDLP-ISR was used to measure the plume of a 6-kW-class single-channel HET called the H6 operated at 300 V and 20 A at 200 kHz. Time-averaged maps of electron density, electron temperature and plasma potential were determined in a rectangular region from the exit plane to over five channel radii downstream and from the centrally mounted cathode radially out to over three channel radii. The power spectral density (PSD) of the time-resolved plasma density oscillations showed four discrete peaks between 16 and 28 kHz which were above the broad breathing mode peak between 10 and 15 kHz. Using a high-speed camera called FastCam imaging at 87,500 frames per second, the plasma oscillations were correlated with visible rotating spokes in the discharge channel. Probes were vertically spaced in order to identify azimuthal plasma transients around the discharge channel where density delays of 14.4  $\mu$ s were observed correlating to a spoke velocity of 1800 m/s in the  $E \times B$  direction. The results presented here are the first to positively correlate observed spokes with plasma plume oscillations that could provide the key to understanding HET operation. High-speed diagnostic techniques enable observation and characterization of the oscillatory nature of HETs which will give critical insight into important phenomena such as anomalous electron transport, thruster operational stability and plasma-spacecraft interactions for future HETs.

## TABLE OF CONTENTS

1. INTRODUCTION.....	1
2. THRUSTER AND EXPERIMENTAL SETUP .....	2
3. HDLP-ISR.....	3
4. AUTOMATED I-V TRACE PROCESSING .....	5
5. PLASMA PLUME PROPERTIES.....	7
6. COMPARISON WITH PREVIOUS RESULTS.....	9
7. ANALYSIS AND DISCUSSION.....	10
8. SUMMARY .....	11
ACKNOWLEDGEMENTS.....	12
REFERENCES.....	12
BIOGRAPHIES.....	13
APPENDIX A .....	15
APPENDIX B .....	16

## 1. INTRODUCTION

Hall Effect Thrusters (HETs) have been under development since the 1960's and first flew in 1971 [1]. They are increasingly used for and considered for a variety of space missions, ranging from satellite station-keeping to cargo transfer for Mars settlement and exploration. Determining the underlying physics of HET operation is critical to increasing efficiency, operational lifetime and spacecraft interaction. End-to-end models of HET operation from first principles do not exist because the question of anomalous electron transport (how so many electrons cross magnetic field lines to reach the anode) is unresolved. Without understanding the full picture of how HETs operate, predictive models of HET operation cannot exist, but are needed to design more efficient and stable thrusters. New thruster designs are verified by expensive and labor intensive 1,000 to 10,000 hour operational life tests, but accurate models could reduce test costs and duration. Verification that the thrusters will operate the same in space as during testing on Earth where the ambient pressures in vacuum chambers can be orders of magnitude higher is very important. All of these issues could be resolved with better understanding of the underlying plasma physics of HET operation to the point of developing first principle, predictive models.

Although HETs are steady state devices, they contain a rich menagerie of plasma oscillations across the frequency

spectrum from 1 kHz - 60 MHz [2] and higher with the breathing mode and rotating spokes modes of primary interest. The so-called breathing mode, a global depletion and replenishment of neutrals akin to the predator and prey models of ecosystems, is commonly observed in HET operation [3–5] and numerical models [6–8] from 15-35 kHz. The spoke modes are azimuthally propagating waves travelling within the channel in the  $E \times B$  direction (axial electric field crossed with the radial magnetic field, counter-clockwise in the H6). Both phenomena are believed to be related to ionization processes and it is uncertain how they interact or feed off each other; however, it is strongly suspected these modes greatly affect anomalous electron transport. Janes and Lowder [9] first discussed oscillating azimuthal electric fields as the cause for spokes and electron transport. McDonald [10–12] and Raiteses et al [13, 14] further explored whether so-called spokes (rotating azimuthal waves) could explain anomalous electron transport, but further conclusive evidence is needed.

Brown [15] showed that at low discharge voltages the thruster would operate either in a high-efficiency (low mean discharge current and oscillations) or low-efficiency (high mean discharge current and oscillations) mode with only slight differences in magnetic field settings, chamber pressure, cathode flow fractions or with externally supplied ambient gas. This transition occurred more readily at higher voltages (closer to flight levels) at lower chamber pressure suggesting that the thrusters may operate differently in the space environment than test facilities on Earth. Further research showed the transition to more efficient operation correlated to stronger spoke modes. [11] Concluding that thruster efficiency and stability are linked to the oscillatory breathing and spoke modes that time-averaged diagnostics cannot detect, the issue becomes how to understand the interaction and dominance of one mode over the other. In order to investigate these phenomena in an effort to build a complete picture of HET operation for system design, high-speed diagnostics are necessary.

The effect of spokes on the transient plume properties is investigated in this work where plasma properties are measured at 100's of kHz and match spoke oscillations observed with high-speed imaging. This paper is meant to initiate a series of publications where the oscillatory nature of HETs were investigated using the new techniques of high-speed probes and imaging described herein. While only one operating condition of one thruster is described here, future publications will expand to different operating conditions and a Nested Hall-effect Thruster (NHT). These experiments are intended to eventually aid in theoretical HET and NHT development by improving our understanding of their fundamental operation, which will have a direct benefit to space system designs that incorporate HETs or NHTs for orbit-raising and/or station keeping.

## 2. THRUSTER AND EXPERIMENTAL SETUP

The ideal test platform for investigating transient plasma properties within an HET is to use a well characterized existing thruster, which is the H6 shown in Figure 1.

### *H6 Hall Thruster*

The H6 Hall thruster is a 6-kW class Hall thruster with a nominal design voltage of 300 V and a 7% cathode flow fraction. It uses a centrally-mounted cathode (mounted coaxially on thruster centerline) with a lanthanum hexaboride ( $LaB_6$ ) insert. The inner magnet coil is continuously wound while the outer coil consists of eight discrete solenoid cores wound in series and separated by 45 degrees. The outer pole is designed such that inside the discharge channel the magnetic field is azimuthally uniform to less than one Gauss.

The H6 was a joint development effort of the University of Michigan, NASA Jet Propulsion Laboratory (JPL) and the Air Force Research Laboratory (AFRL) at Edwards AFB, and a separate copy of the thruster is maintained at each institution. It is notable for its high total efficiency, 64% at nominal 300 V, 20 mg/s (6.1 kW) operation and 70% at 800 V, 6 kW operation [16]. Slightly different nominal operating conditions are used between institutions. At the University of Michigan work by Reid, Shastry, Huang and McDonald studied operation between 5 and 30 mg/s flow rates, but primarily focused on 20 mg/s for approximately 6 kW operation at 300 V. Work by Hofer at the JPL has tuned the H6 to even discharge currents and power levels, i.e., 20 A for exact 6 kW operation at 300 V. For xenon these operating conditions vary only by a few percent in current or mass flow rate (1 mg/s Xe  $\sim$  1 A), but peak magnetic field strengths between the two cases may vary by up to 15%. At the 300 V, 20 mg/s Michigan operating condition the H6 has a 20.3 A discharge current, produces 397 mN of thrust at a specific impulse of about 1900 s [17]. At the nominal 300 V, 20 A, 6 kW JPL condition, the specific impulse is 1950 s with a thrust of 401 mN [16].

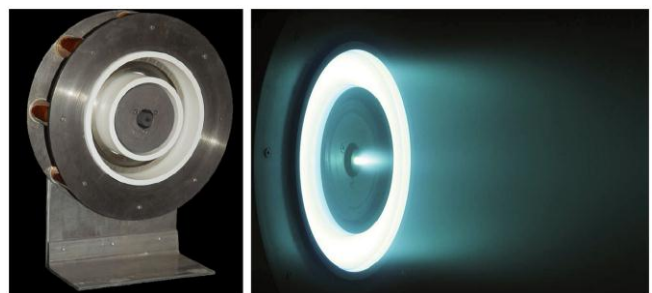


**Figure 1 The H6 6-kW Hall thruster, left, before first firing in 2006; right, at nominal 300 V, 20 mg/s (20.3 A) operating conditions. Images courtesy of Reid [17].**

Since first firing in 2006 the H6 has been well characterized by a variety of diagnostic and modeling techniques at Michigan, JPL and AFRL. Six experimental doctoral dissertations have focused on the thruster to date, [10, 17–

21] which have spawned numerous associated conference and journal articles. Modeling of the H6 has been performed using the hybrid Particle-In-Cell (PIC) simulation HPHall-2 [22] and the more recently developed fluid code Hall-2De [23]. The H6 is a well characterized HET with multiple references for steady-state values and provides an ideal platform for high-speed investigations of oscillatory plasma phenomena undoubtedly present.

The xenon propellant is delivered to the HET using MKS and Alicat Scientific MC Series mass flow controllers through electro-polished stainless steel lines. Mass flow calibration takes place through a Bios Definer 220M DryCal system plumbed in parallel to the anode and cathode feed lines with an accuracy of 1% of reading between 50-5000 sccm. Mass flow calibrations are taken for each mass flow controller at several flow rates and a linear fit is used to determine the flow produced at any arbitrary set point. The AC component of the thruster discharge current was measured with a Tektronix TCP 312 split-core Hall current sensor with a DC-100 MHz bandwidth. The signal was measured on the discharge current line external to the chamber and was acquired simultaneously with HDLP-ISR signals on the same Data Acquisition (DAQ) system described later.

#### Facility Information

Testing occurred in the Large Vacuum Test Facility (LVTF) of the Plasmadynamics and Electric Propulsion Laboratory (PEPL) at the University of Michigan. The LVTF is a 200 m<sup>3</sup> stainless steel-clad vacuum chamber 9 m long and 6 m in diameter. Rough vacuum is achieved with two 2000 CFM blowers backed by four 400 CFM mechanical pumps with a final base pressure in the low 10<sup>-7</sup> Torr achieved by seven CVI TM-1200 re-entrant cryopumps with LN<sub>2</sub> baffles and a nominal pumping speed of 500,000 L/s on air or 240,000 L/s on xenon. During thruster operation the chamber pressure was 1±0.1x10<sup>-5</sup> Torr, corrected for xenon, as measured with a nude and external ion gage.

#### Motion Stages

Two perpendicularly-mounted motion stages, one radial and one axial, were used to acquire plasma plume data in a 2-D plane. The radial stage is a 1.5 m long Aerotech ATS62150 ball screw stage driven by a stepper motor as shown in Figure 2. It is used in open loop position feedback mode with a 15 V string potentiometer to monitor the radial stage position during movement. The axial stage is a 0.5 m long Parker Trilogy T2S I-Force Ironless Motor Positioner, a linear motor capable of a maximum of 6 g acceleration and 5 m/s velocity. This stage is better known as the High-speed Axial Reciprocating Probe (HARP) and is used for axial injection of plasma probes into the thruster plume as shown in Figure 2. It operates in a closed loop position feedback mode with 5 μm resolution Renishaw LM10 encoder. Both stages are operated by Aerotech motion controllers, an Aerotech MP10 for the radial stage and an

Aerotech CP20 for the axial HARP stage, that are both automated from LabView.

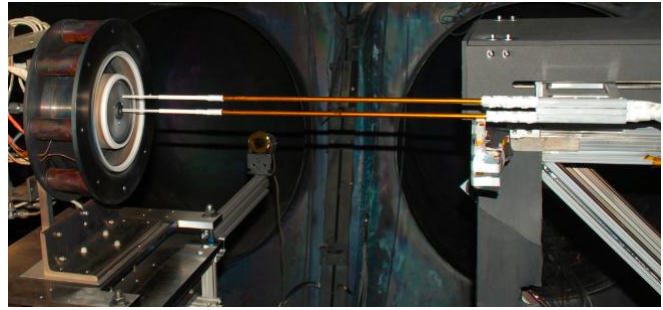


**Figure 2 HDLP-ISR mounted on HARP shown at full extension to the discharge channel exit plane on cathode centerline.**

#### High-Speed Imaging

High-speed imaging was acquired with a Photron SA5 FASTCAM with a Nikon ED AF Nikkor 80-200mm lens at its maximum aperture f/2.8. The SA5 is capable of up to 1,000,000 fps with 128x16 pixel resolution, but was used at 87,500 fps with 256x256 pixel resolution for this testing. The Fourier analysis techniques described by McDonald [12, 24] were applied to the FastCam videos to determine breathing and spoke mode frequencies.

### 3. HDLP-ISR

The first technique for measuring plasma properties was the electrostatic probe developed by Irving Langmuir circa 1924 [25] and remains one of the most fundamental diagnostics for plasma measurements today. The Langmuir probe consists of a small metallic electrode, usually a wire, inserted into a plasma and biased at various voltages to measure the current response known as I-V traces (for current-voltage). The plasma properties including density, plasma potential and electron temperature or electron energy distribution function (EEDF) can be calculated with the voltage-current traces as discussed in Section 4. Due to their ubiquitous use, Langmuir probe theory has enjoyed considerable attention within the literature [25–32] so only the relevant basics will be recapitulated here.

#### High-speed Dual Langmuir Probe (HDLP)

Langmuir probe voltages can be varied slowly to generate time averaged measurements of plasma properties or can be swept fast to measure plasma transients, exemplified by [3] where the plasma properties and EEDFs were measured at a remarkable 400 kHz. Such measurements were made possible using the High-speed Dual Langmuir Probe (HDLP) [33–35] developed by Lobbia shown schematically in Figure 3. The HDLP uses an active and null probe to cancel the capacitive current,  $I_{cap}$ ,

$$I_{cap} = C \frac{dV}{dt} \quad (1)$$

generated by rapid, high amplitude (i.e. large  $dV/dt$ ) voltage sweeps with the resulting plasma currents measured by a wideband current transformer manufactured by Pearson Electronics (Pearson coil) in the vacuum chamber. However, the current transformer cannot measure DC currents so either a shunt resistor must be used or another reference to the low frequency current is necessary.

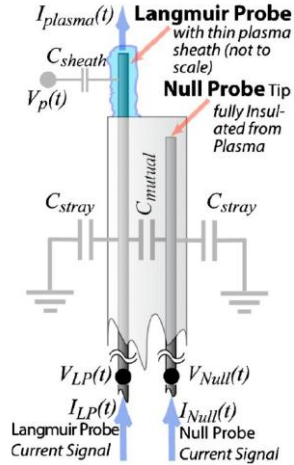


**Figure 3 Diagram of HDLP adapted from Lobbia [34] showing active and null probes with capacitances represented schematically.**

#### Ion Saturation Reference

The null probe in the HDLP is meant to cancel capacitive current due to stray and line capacitance as well as cancel noise incident on both probes, but the plasma sheath capacitance is of order  $10^3$ 's pF [36]. Consider a  $\pm 50$  V, 200 kHz sine voltage signal, the maximum  $dV/dt$  yields a peak capacitive current from (1) of 630  $\mu$ A assuming a 10 pF sheath capacitance. This current overwhelms the plasma current in the ion saturation region where the current is also of the order 100  $\mu$ A. Therefore, an alternative, reliable measurement of the ion saturation current is needed that fluctuates with the plasma. The solution is to use a second Langmuir probe several millimeters or more away, far enough not to disturb the swept probe, but close enough to maintain reasonable spatial resolution. This probe is maintained at a continuous negative bias for time resolved ion saturation measurements. Additionally, this probe is able to provide the ion saturation portion of the I-V trace which acts as the DC reference necessary for the HDLP probe which was not provided by the current transformer. The resulting system is hereby known as the HDLP-ISR.

#### Temporal Limits

Lobbia discussed the temporal limits of Langmuir probes in [34] and only the important results will be discussed here. A full set of frequency limitations were developed for Langmuir probe measurements based on plasma properties and probe characteristics. As summarized in Table 1 of [34], the near-field region for a typical HET has the

frequency limits in the single to hundreds of MHz, which are well above the sweep frequency used here of only 200 kHz. The stray capacitance is mitigated by the HDLP configuration which uses a null probe. The mutual capacitance limitation is avoided with the HDLP-ISR because shunt resistors are not used since the ISR provides the DC reference.

#### HDLP-ISR Hardware

A 200 kHz sinusoidal signal generated by a Tektronix AFG3101 is amplified using a Krohnkite 7500 wideband power amplifier capable of DC to 1 MHz output with  $\pm 200$ V range to generate the probe bias. The DAQ system consists of eight channels sampled at 180 MHz with 16-bit AlazarTech ATS9462 digitizers. The HDLP current is measured with the active and null probe lines wound in opposite directions through a model 6585 Pearson coil protectively mounted inside LVTF with less than 2 m of cable length from the probe tip to current measurement location to minimize capacitance. The ISR current is measured external to LVTF across a shunt resistor through an Analog Devices AD 215 120 kHz low distortion isolation amplifier where the 2  $\mu$ s offset has been accounted for. The 2  $\mu$ s offset was specified on the data sheet and verified using the AFG3101 and a Tektronix digital oscilloscope. The probes consist of 0.38 mm diameter pure tungsten wire with 3.2 mm exposed for the active HDLP probe and 3.3mm exposed for the ISR probe.

In Figure 2, the bottom probe was the HDLP and the top probe was the ISR, which were separated by 26.5 mm. This gap is larger than preferred for HDLP-ISR operation since the ISR probe will be sampling a different segment of plasma and will not provide the correct ion saturation current to correct the HDLP trace. However, the fluctuations in ion saturation current are  $10^3$ 's to  $10^4$ 's of  $\mu$ A and the rest of the I-V trace is  $10^3$ 's to  $10^4$ 's mA as seen in Figure 4 so the effect on electron density calculations is negligible.

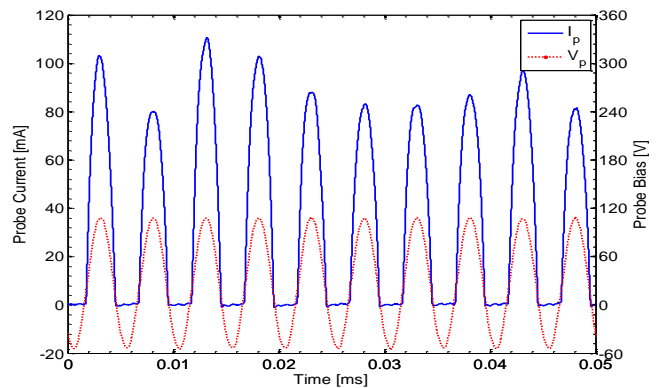


**Figure 4 Example time history of probe bias and probe current for the first 0.05 ms of the channel centerline ( $R/R_{channel} = 1$ ) shot. Each half-cycle of the probe bias was "chopped" into an individual I-V trace for calculating plasma properties.**

The voltage range swept for the HDLP varied based on radial location, but in general ranged from -50 to +150 V around the floating potential. At each radial location, the probes were first injected to generate a floating potential profile for each shot. The probes were subsequently injected again while sweeping around the floating potential. Figure 4 shows an example segment of the time history trace for the probe bias and probe current. Note that each half-cycle of the probe bias and corresponding probe current form one complete I-V trace.

#### 4. AUTOMATED I-V TRACE PROCESSING

As will be shown later for this testing, time-resolved plasma measurements require processing of  $10^5$  to  $10^6$  I-V traces, which is impractical to do by hand. Therefore, an automated technique that was initially developed for HDLP [3, 33, 35] has been adapted for HDLP-ISR automated I-V trace processing. The premise of HDLP analysis is the standard collisionless, thin-sheath Langmuir probe theory which has been discussed in literature [25–32] with the basics outlined below. Note that all electron temperatures,  $T_e$ , in the equations below, are in eV. The criteria for thin-sheath is the probe radius to Debye length ( $\lambda_D$ ) should be greater than 1. A typical I-V trace for a cylindrical Langmuir probe is shown in Figure 13 of Appendix A and consists of three regions:

1. Ion saturation region where the probe is biased negative to repel most electrons and collect ions.
2. Electron retarding region approximately between the floating potential and the plasma potential where the probe is collecting both ions and electrons.
3. Electron saturation region where the probe is biased positive with respect to the plasma potential to repel ions and collect electrons.

##### Probe Current and Electron Density

The ion current to a probe accounting for the Bohm criteria and assuming only singly charged ions is [26]

$$I_+ = 0.61n_e e A_s v_B \quad (2)$$

where  $n_e$  is the plasma density outside of the sheath,  $e$  is the fundamental charge,  $A_s$  is the sheath area and  $v_B$  is the Bohm velocity given by

$$v_B = \sqrt{eT_e / m_i} \quad (3)$$

The electron current to a probe biased at  $\phi$  in the electron retarding region, assuming a Maxwellian velocity distribution, is

$$I_e = -\frac{1}{4} A_{probe} n_e e v_{th} \exp\left[\frac{\phi - V_p}{T_e}\right] \quad (4)$$

where  $A_{probe}$  is the area of the probe,  $V_p$  is the plasma potential and  $v_{th}$  is the thermal velocity

$$v_{th} = \sqrt{\frac{8eT_e}{\pi m_e}} \quad (5)$$

The electron density can be calculated from (4) with the electron saturation current,  $I_{e_{sat}}$ , the point at which the probe enters electron saturation

$$n_e = \frac{I_{e_{sat}}}{0.25 A_{probe} v_{th}} \quad (6)$$

##### Plasma Potential

While not as precise as emissive probes, plasma potential can be determined from Langmuir probe I-V traces by identifying the “knee” in the curve identifying the transition from electron retarding to electron saturation. As noted frequently in the literature, determining the plasma potential from the “knee” in the I-V curve is imprecise because the “break in the characteristic is frequently far from abrupt,” [31] especially for a cylindrical probe where the transition from electron retarding to electron saturation is gradual even in the best of circumstances (c.f. Fig. 5 from [25]).

The slope of the electron current,  $dI_e/d\phi$ , is exponentially related to the probe bias and  $T_e$  as seen from the derivative of (4); therefore  $dI_e/d\phi$  should be increasing with  $\phi$  until the electron saturation region is reached where the slope will then decrease significantly. Therefore, the peak in  $dI_e/d\phi$  is a reasonable measure for plasma potential [30, 32]. As noted in [37], this method tends to under-predict the plasma potential where +2/-1 V error was assumed on  $V_p$  calculations in that work. An example of detecting the  $dI_e/d\phi$  peak value is shown in the lower-left plot of Figure 13 in Appendix A.

Testing with various methods of fitting lines to the electron retarding and electron saturation regions to determine  $V_p$  from the intersection yielded unsatisfactory results because the electron saturation region was not well represented by a straight line. Therefore, the method of determining  $V_p$ , and hence  $I_{e_{sat}}$  from the peak of  $dI_e/d\phi$  will be employed in this work. The electron saturation current is the electron current at  $V_p$  and is then used to calculate  $n_e$  from (6). Using this technique yielded more consistent results, which is critical for autonomous analysis of hundreds of thousands of I-V traces for time-resolved plasma property calculations.

## Electron Temperature

The electron temperature with an assumed Maxwellian energy distribution for traditional, collisionless, thin-sheath Langmuir probe analysis is found from the inverse of the slope of  $\ln(I_e)$  versus  $\phi$  in the electron retarding region from the floating potential,  $V_f$ , to  $V_p$  (from taking the natural log of (4)). However selecting all points between  $V_f$  and  $V_p$  will include the gentle transitions (the gradual “knee”) between the regions and thus skew the slope of the line, so only the linear points in the center between  $V_f$  and  $V_p$  should be selected. This process is simple to perform manually, but to automate analysis for 100,000’s I-V traces, a reliable selection method is necessary. The slope of a line can be determined from as few as two points, so the selection criteria for what datum points to include from the tens to hundreds in the electron retarding region during a single I-V sweep could be stringent. However, the maximum number of reliable points are desired because Lobbia [35] points out the non-systematic  $T_e$  uncertainties are reduced by a factor of  $1/\sqrt{N_{T_e}-1}$  where  $N_{T_e}$  is the number of I-V points used to calculate  $T_e$ . Before a point selection method can be considered,  $V_p$  and  $V_f$  need to be determined.

The floating potential,  $V_f$ , is the point of zero crossing for the I-V trace; however, the ion saturation current portion of the trace is so small compared to the electron retarding and electron saturation currents that noise often corrupts the signal introducing significant error in determining the probe bias for zero current. This is a peculiarity to high speed Langmuir probe data because the floating potential is the characteristic typically easiest to measure with low speed I-V sweeps. For the HDLP-ISR system, the purpose of the ISR reference is to give a reliable ion saturation current to calculate ion density and compensate for this noise, but since the ISR bias is not varied  $V_f$  cannot be determined reliably.

The total current to the probe is the sum of (2) and (4). When the probe is at  $V_f$  the total current is zero because the ion and electron currents balance. Equating (2) and (4) and assuming  $A_s = A_{probe}$  for thin sheath yields a relationship for  $V_f$ ,  $V_p$  and  $T_e$  [29, 31] where the coefficient has been calculated for xenon

$$V_p = V_f + T_e \ln \left[ \frac{1}{0.61} \sqrt{\frac{m_i}{2\pi m_e}} \right] \approx V_f + 5.8T_e. \quad (7)$$

The importance of equation (7) is to show that the floating potential should be several electron temperatures below the plasma potential.

The value of  $dI_e/d\phi$  up to electron saturation should be approximately 0 for the entire ion saturation region since negligible electron current is collected and then from (4) it should become exponential after  $V_f$  up to  $V_p$  and  $I_{e,sat}$ . The lower left plot in Figure 13 in Appendix A shows this to be

accurate except close to  $V_p$ , which is clearly no longer exponentially increasing. Very near the plasma potential the I-V curve does not follow the simple, collisionless, thin-sheath model. A consistent and robust method for setting the lower bound of points to select for the  $T_e$  calculation is when  $dI_e/d\phi$  rises above some constant threshold value, which should be somewhat close to  $V_f$ . Subsequently, select a certain fraction of points between that threshold value and  $V_p$  starting with the threshold value. This will ensure that no points are selected near the gentle transition region to electron saturation near  $V_p$ . An example of this threshold value is shown in the lower-left plot of Figure 13 in Appendix A. To illustrate this concept, consider a single I-V sweep with 50 datum points between  $V_f$  and  $V_p$ . Using a threshold value of 25% and an inclusion fraction of 40%, 15 of those points would be used to fit a straight line whose slope yields the electron temperature.

A parametric study was conducted by varying the threshold value (percentage of  $[dI_e/d\phi]_{peak}$  to begin selecting points) and the fraction of points to select between that threshold value and  $V_p$  as shown in the time-averaged results of Figure 5. The results were insensitive ( $T_e$  varying by less than  $\sim 0.1$  eV) to the threshold value as long as it was 15-33% of  $[dI_e/d\phi]_{peak}$ , which according to (7) should be  $\sim 1-2 T_e$  above  $V_f$ . Selecting a fraction of points between the threshold value and  $V_p$  was insensitive until the fraction was large enough (75-100%) to include the electron saturation transition. This caused the electron temperature to be artificially increased as seen in Figure 5 by decreasing the slope of the fitted line. In fact, the values for threshold 20/fraction 50, threshold 25/fraction 40 and threshold 33/fraction 33 all lie on top of one another. Therefore, a threshold value of 25%  $[dI_e/d\phi]_{peak}$  was the start and 40% of the  $\ln(I_e)$  points from there towards  $V_p$  were selected to conduct a linear fit to determine  $T_e$  with an example shown in the upper-right plot of Figure 13 of Appendix A.

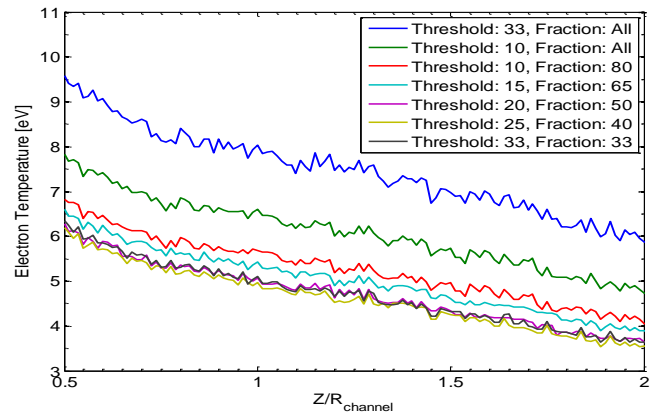


**Figure 5** Parametric variation of the threshold value and fraction of points used in calculating  $T_e$  for the time-averaged results at  $R/R_{channel} = 1$  and a range  $Z/R_{channel}$  from 0.5 to 2.

### Quality Control and Data Auditing

Figure 13 of Appendix A shows a typical I-V trace and resulting analysis. The  $[dI_e/d\phi]_{peak}$  is well defined and is clearly below the peak probe bias which ensures electron saturation is achieved. Also shown is the linear fit to the selected electron retarding region to calculate electron temperature. The validity of results from automated data processing can be questionable without adequate quality controls in place to build confidence. In order to maximize the reliability of results from automated data processing, automatic reject criteria were developed for each I-V trace:

1. If  $R_p/\lambda_D \leq 1$  then the probe was no longer in thin sheath regime.
2. If the potential for the  $dI_e/d\phi$  peak was within the last 10% of the I-V sweep, then the probe bias may not have reached plasma potential and entered electron saturation.
3. If the  $R^2$  value for the linear fit to  $\ln(I_e)$  versus  $\phi$  was less than 0.990, then the electron energy distribution may not have been Maxwellian or the data contained noise.

Finally, a manual auditing process was also used whereby traces were selected at random or odd features were examined on a trace-by-trace basis to determine regions of rejected data. An entire radial shot was rejected if the ISR current was of the wrong sign, which most likely resulted from experimental setup and operator error where the ISR bias was not applied. Additional entire radial shot rejection criteria were plasma properties not conforming to adjacent radial shots. These situations only occurred in 4 out of 61 shots.

## 5. PLASMA PLUME PROPERTIES

The plasma plume properties are determined in multiple steps. Each injection of the probe into the plasma plume is analyzed individually to generate time-averaged and time-resolved quantities. The time-averaged quantities are stitched together to create 2-D contour maps of the plasma plume properties.

### Single HLDP-ISR Shot

The HDLP-ISR was swept using a 200 kHz sine wave with each cycle completing two I-V sweeps (one up-sweep and one down-sweep). Each HARP injection lasted approximately 420 ms, which yielded approximately 168,000 I-V sweeps per radial location. Given the sinusoidal velocity profile of the HARP, the “dwell time” at each axial location was not constant. For the time averaged results, all sweeps within 1 mm of travel were averaged together to give one I-V trace to represent that point in the R-Z plane. This represented 100’s to 1000’s of I-V traces for each 1 mm of axial travel. Each I-V trace was processed using the automated algorithms and manual auditing

described in Section 4 to generate time-averaged plasma properties as a function of axial distance for each radial location measured.

### Time-Averaged Plasma Property Contour Maps

The probes were injected 61 times at varying radial locations as shown in Figure 6 to measure plasma properties in a 2-D plane. Combining each individual probe injection yielded 2-dimensional contour maps of time-averaged plasma properties in the R-Z plane. The spatial domain extended from cathode centerline radially out to over 3 channel radii and from the channel exit plane downstream to over 5 channel radii. Slight smoothing was done for each injection and for the 2-D contours, although some small noise still remained which can be seen in the example electron temperatures of Figure 5. The jagged edges of contour lines or small “islands” of increased or decreased plasma properties seen in the contour plots are due to such noise in the results and do not represent time-resolved plasma oscillations. A quadrant of the H6 is shown to scale at the contour plot top in order to show cathode and discharge channel locations for reference. All locations and lengths are non-dimensionalized by the discharge channel centerline radius,  $R_{channel}$ . The results are shown in Figure 14, Figure 15 and Figure 16 of Appendix B for electron temperature, plasma potential, electron density and ion density, respectively.

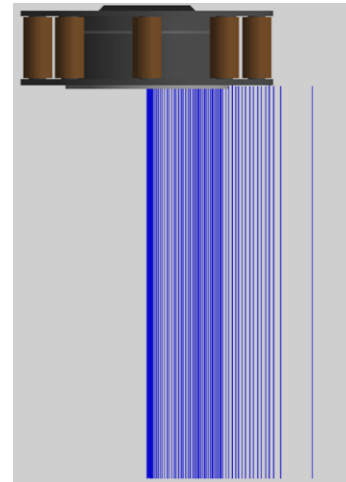


**Figure 6 Top view of H6 (discharge channel not visible) with blue lines representing radial locations of probe injections with the HARP. Note the increased resolution (more injections per radial length) over the cathode on thruster centerline and over the discharge channel.**

Figure 16 of electron density shows a slight wave in the radial direction making the properties appear to “flicker” back and forth slightly like a flame. This is likely due to probe movement side-to-side during injection on the HARP of approximately  $\pm 2$  mm. As seen in Figure 2 the probes have a very long aspect ratio and likely did not shoot into the thruster without latitudinal swaying. During injection, a significant torque was applied to the probe array from the

HARP while accelerating them towards the thruster. Close inspection of the time-averaged spatial plasma properties data where the radial shots over the discharge channel were spaced 2 mm apart indicated that the probes did not completely sway more than one radial increment, therefore a conservative estimate of 2 mm is assumed for the probe location uncertainty both horizontally and vertically.

Figure 14 shows the electron temperature contours with a peak near the channel exit as expected. An interesting observation are the streams of hotter electrons emanating from both poles (regions on the thruster face outside the channel) extending out at approximately  $5^\circ$  from the thruster axis. These are close to the magnetic field lines (not shown) in the far field region and will be investigated further in future work.

The plasma potential contours in Figure 15 also show the expected increase in plasma potential near the channel exit. The plasma potential is higher for  $R/R_{channel} < 1$  (the plume region within the discharge channel diameter) and decreases significantly outside the channel diameter. Figure 15 has the same shape and similar magnitude as figure 6.43 of Jameson [18] and Figure 5-12 (top) of Reid. [17] Further comparison with Jameson's and Reid's results will be discussed in the next section.

Figure 16 shows the electron density which is also peaked over the discharge channel at  $5 \times 10^{17} \text{ #/m}^3$ . The electron density is very low near the inner pole and of course is low outside of the channel radius. The general shape of the contours show that as plasma emanates from the entire discharge channel the plasma streams converge towards, but do not cross, thruster centerline.

#### Time-Resolved Plasma Properties

Every two traces were averaged together to yield time-resolved plasma properties during each injection. This technique reduced the rate of I-V traces (hence plasma properties) to 200 kHz but averaged out slight differences between up-sweeps and down-sweeps. With approximately 168,000 total I-V traces per injection this resulted in 84,000 I-V traces to calculate plasma properties every  $5 \mu\text{s}$ . The same technique used for time-averaged plasma property calculations of automated I-V analysis with manual audits was employed as described in Section 4.

A common sense check was performed whereby the time-resolved properties ( $n_e$ ,  $T_e$ ,  $V_p$ ) were averaged together for each millimeter of HARP travel and compared to the time-averaged results obtained by averaging the I-V traces together before calculating plasma properties. Figure 7 shows an example of this comparison for the radial location of  $1.25 R_{channel}$  and the time selected of 227 ms corresponding to an axial location of  $2.13 R_{channel}$  during injection. As expected, the results are very similar indicating that the time-resolved plasma properties are indeed oscillating about the calculated time-averaged values. The time-averaged plasma properties for the time

segment shown in Figure 7 was calculated from over 250 individual I-V sweeps averaged together to create one I-V trace. The time resolved points in Figure 7 are at 200 kHz because every other trace was averaged together.

The comparison of time-averaged to the average of time-resolved did not correlate well within  $\sim 1/4 R_{channel}$  of the cathode or channel exit where the I-V traces became very distorted due to noise. In those situations, the time-averaged values maintained better integrity since over 500 sweeps were averaged together to calculate the plasma properties which was able to average out the noise to generate a clean I-V trace. Therefore, the time-resolved data near the cathode and channel exit were less reliable.

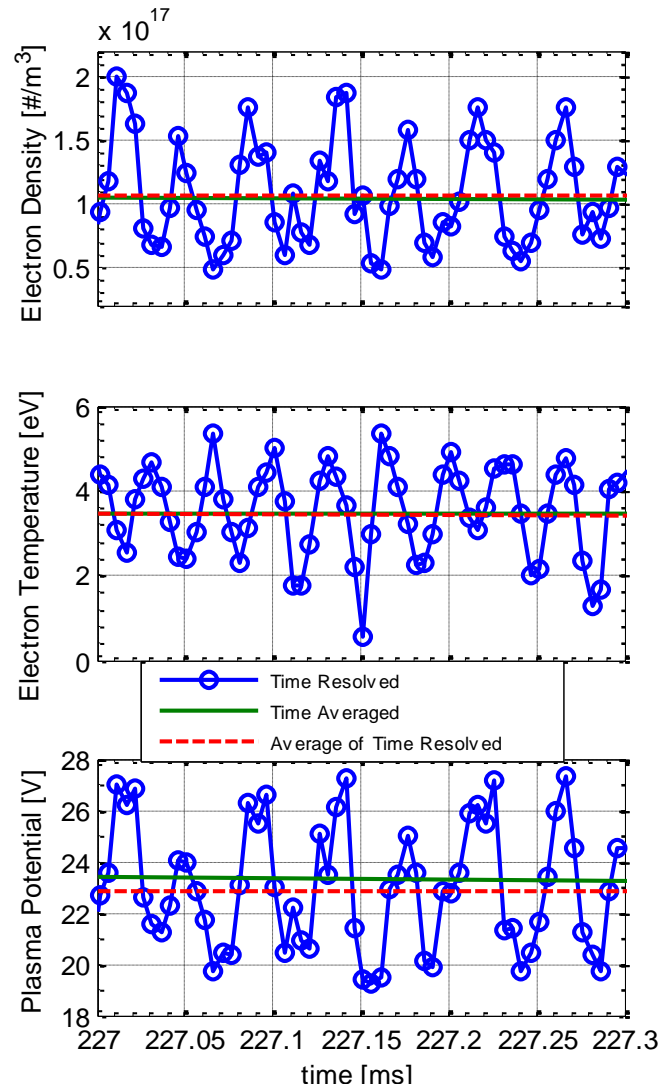


**Figure 7 Comparison of time-resolved and time-averaged plasma electron density, electron temperature and plasma potential for  $R/R_{channel} = 1.25$  and time 227.0 to 227.3 ms which corresponds to an axial position of  $Z/R_{channel} = 2.13$  during probe injection.**

Simply counting the number of cycles over the 0.3 ms shown in Figure 7 yields estimated 20-30 kHz plasma



property oscillations. This also confirms that measuring plasma properties at 200 kHz is well above the Nyquist criteria for the 10's kHz oscillations present and meaningful time resolved plasma property data is present.

### Uncertainty Analysis

A critical component of any experimental investigation is an uncertainty analysis of measurement accuracy (error with respect to true value) and precision (error in repeatability). While Langmuir probe measurements are not renowned for their accuracy, the measurements presented here appear precise as demonstrated in the time-resolved plasma properties of Figure 7. If the oscillations were entirely due to inaccurate measurements, then the points would simply oscillate approximately every other point about the mean bouncing up and down. The time-resolved data shows the properties appear to have a sinusoidal nature with three to four points together above or below the mean before transitioning. As shown in Figure 7, the electron temperature and the plasma potential oscillate by less than 2 eV and 4 V, respectively. If the uncertainty on the measurements were conservatively estimated to be 1 eV and 3 V, which are reasonable values for Langmuir probe measurements, then the time-resolved data would be rendered nearly meaningless. Therefore it is important to distinguish the uncertainty in the mean values (time-averaged) and uncertainty in the oscillatory values (time-resolved).

During development of the HDLP [35], Lobbia included a detailed discussion and analysis of error. Comparative measurements were made of averaged results from rapidly swept probes (100 kHz) to slowly swept probes (100 Hz) with a difference in measured plasma properties of approximately 23%. Error analysis of the thin sheath relations yielded approximate errors of  $\partial n_e/n_e \approx \partial T_e/T_e \approx 10\text{-}20\%$  and  $\partial V_p/V_p \approx 10\text{-}40\%$ ; however, these are dependent on the local plume conditions tested in [35]. This represents the error in time-resolved values to time-averaged values (error in oscillatory values to the mean). As noted in the numerous Langmuir probe theory reviews [25–32], interpretation of I-V traces to plasma properties is difficult and error prone. Sheath limited electrostatic probe theory has an error on the order of 50% [35] with electron density possibly in error by a factor of 2 or 3 [38]. Based on the preceding discussion, the uncertainty in time-resolved, oscillatory plasmas value to the local mean value will be assumed as 25% and the uncertainty in time-averaged, mean value of a plasma property to the true local value will be assumed as 50%.

## 6. COMPARISON WITH PREVIOUS RESULTS

The next check is to compare the time-averaged values with previous results for the thruster operating at or near this condition. The experimental thesis of Jameson [18] characterized the sensitivity of H6 efficiency which included plume maps at the 300 V, 20 A operating condition (Section 6.2.1). Time-averaged measurements were made

of plasma potential and electron temperature using emissive probes and Langmuir probes. The electron temperature and plasma potential in Figure 7 can be compared with Figure 6.44 and 6.40 in [18], respectively. For the same location within the plume, the electron temperature is 4 eV in Figure 6.44 of [18] and the time-averaged quantity in shows 3.5 eV. Similarly, the plasma potential is 22–23 V in Figure 6.40 of [18] and the time-averaged quantity in Figure 7 shows 23 V. However, the time-resolved quantities in Figure 7 show the electron temperature and plasma potential are oscillating a few eV and several volts, respectively, about those average values.

The electron temperature (Figure 8 top) on cathode and channel centerline can be compared with Figure 6.45 and 6.46 of Jameson [18], respectively. Figure 6.46 for channel centerline electron temperatures shows a distinct hump in  $T_e$  around  $Z/R_{channel} = 1$ . Close inspection of Figure 8 also shows a slight bump from 1 to 1.5  $Z/R_{channel}$  before settling out to the far field temperature of 2.5 eV. The near field temperature of just over 12 eV is within 1 eV of the value reported by Jameson. Figure 6.45 shows cathode centerline electron temperature with a peak near 8.5 eV inside  $Z/R_{channel} = 1$  before decreasing while Figure 8 shows the peak of 7 eV just inside  $Z/R_{channel} = 1$ . The far field of Figure 6.46 and 6.45 are 4 eV while in Figure 8 for the same location the electron temperature is 3.2 eV. Therefore, the same trends are observed between Jameson's research and this investigation with slight differences in magnitudes that are within 1 eV.

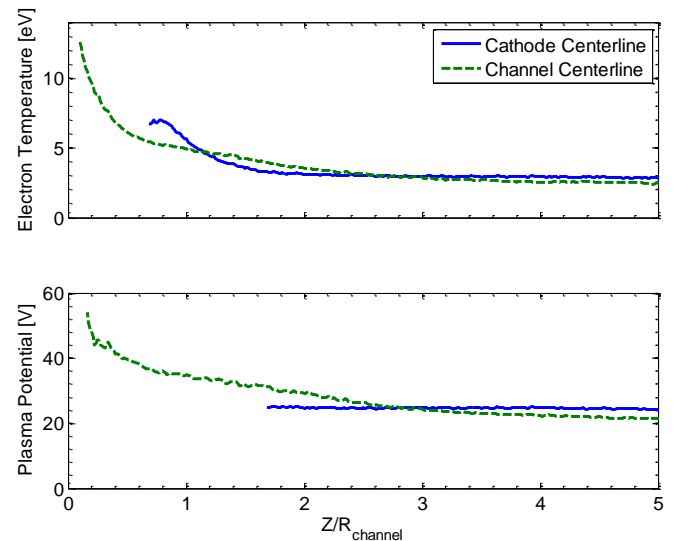


**Figure 8 Electron temperature (top) and plasma potential (bottom) on cathode centerline (solid blue) and channel centerline (dashed green) for comparison with Jameson [18] and Reid [17].**

The plasma potential (Figure 8 bottom) on cathode and channel centerline can be compared with Figure 6.41 and 6.42 of Jameson [18], respectively. The far field of Figure 6.41 and 6.42 are between 20 and 25 V which is close to the far field in Figure 8 of 25 V. The near field for channel

centerline in Figure 8 is 54 V while in Figure 6.42 it is only 38 V. Reid [17] also measured plasma potential and electron temperature using emissive and Langmuir probes, but at 300 V and 20 mg/s flow which is not exactly the test case here. Based on Figure 7-20 of Reid for 20 mg/s a plasma potential on channel centerline of 40-50 V peak would be expected at  $Z/R_{channel} = 0.16$  (minimum value in Figure 8). Again, similar trends are observed but the plasma potentials in Reid and this investigation are higher than Jameson.

## 7. ANALYSIS AND DISCUSSION

The value of high speed probes is displayed by the ability to extract oscillatory plasma behavior through PSD analysis or transient properties through time history analysis.

### Power Spectral Density (PSD)

In order to further investigate the plasma oscillations evident in Figure 7, the PSD was calculated for both ion and electron density and compared to discharge current for channel centerline ( $R/R_{channel} = 1$ ). Approximately 2/3 of the time history signal was used for the PSD shown in Figure 9, which was a majority of the axial extent. However, even using a small selection of time history yields the same results.

The distinguishing features in Figure 9 are the frequency peaks in both ion and electron density. The peaks correspond to oscillations at 16, 20, 24 and 28 kHz, which agrees with the rough observation in Figure 7. What is also immediately obvious is the lack of corresponding peaks in the thruster discharge current, which only displays the broad breathing mode peak between approximately 10-15 kHz. Previous high-speed investigations [3] on different HETs have noted the electron density oscillations to follow the discharge current (with an appropriate time-of-flight delay), which showed a more distinctly peaked breathing mode. However, those measurements were farther out in the plume and did not approach the channel exit plane as closely as this investigation.

In order to confirm the presence of peaked frequency oscillations differing from the breathing mode, a PSD was generated with the FastCam in Figure 10 which only analyzes the azimuthally varying light intensity [12, 24] and does not calculate plasma properties. The frequencies of a 2-D PSD correspond to a local frequency that would be measured in a fixed location within the thruster. The  $m = 0$  mode in Figure 10 corresponds to the breathing mode, which is a global brightening and dimming of the entire thruster discharge channel. The shape matches the discharge current in Figure 9 (note the ordinate axis units are arbitrary) as expected from previous investigations [24]. The modes for  $m \geq 1$  correspond to the number of spokes present. As seen in Figure 10 the modes can “smear” into each other due to the turbulent discharge [24] where they exhibit the same peaks, so the important peak for each mode is the value where it dominates:  $m = 5$  peaks at 16 kHz,  $m =$

6 peaks at 20 kHz,  $m = 7$  peaks at 23 kHz and  $m = 8$  peaks at 28 kHz. Based on these frequencies and modes using the analysis from [24], the expected spoke velocity (the linear speed with which the spoke is traveling azimuthally around the channel) is 1600-1800 m/s.

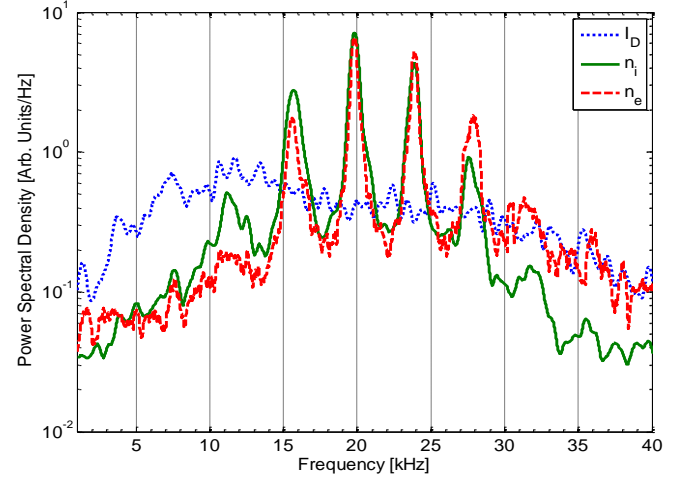


**Figure 9 Power Spectral Density for thruster discharge current, ion density and electron density for  $R/R_{channel} = 1$ . Frequency peaks match those identified with the FastCam in Figure 10.**

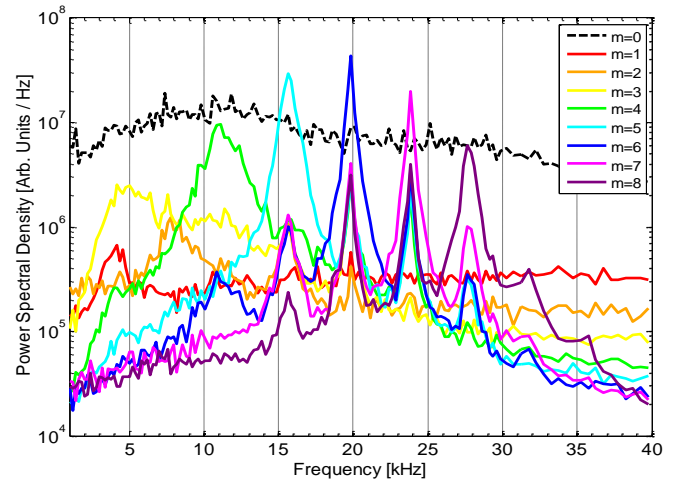


**Figure 10 Power Spectral Density for plasma oscillations from FastCam based on the analysis techniques described in [11, 12].**

As shown in Figure 10, the FastCam detected the exact same frequency peaks as noted in the ion and electron density. This exciting result provides the first confirmation that observed spokes have a direct correlation to transient plasma properties in the thruster downstream plume. One possible interpretation is that the spokes (bright regions in the discharge channel) correspond to increased ionization zones and increased plasma density moving azimuthally in the discharge channel. These regions of increased density

would produce density peaks that would then move axially outward (downstream) into the plume where probes in a fixed plane would measure them as plasma oscillations but could not determine whether they were generated from the global breathing mode (axial oscillations) or from azimuthally moving spokes (azimuthal oscillations). If the spokes are indeed azimuthally moving regions of increased ion density, then azimuthally spaced probes should detect a time of arrival difference in density measurements that would correlate to the spoke velocity.

### Time Delay from Spaced Probes

Vertically spaced probes as seen in Figure 2 were used to identify azimuthal plasma waves by identifying signal delays via cross correlation. The probes were not perfectly azimuthally spaced with the bottom probe on channel centerline ( $R/R_{channel} = 1$ ) and the top probe at a radius of  $R/R_{channel} = 1.05$ , but the difference was negligible so the probes are approximated as azimuthally spaced by  $19^\circ$ . In order to investigate azimuthal density delays, the probes shown in Figure 2 were both operated in ion saturation instead of the bottom as an HDLP and the top as ISR; although different techniques for biasing and sweeping produced similar results. This enabled time delay measurements of the signals where a clear time delay can be identified. The top plot of Figure 11 shows a normalized ion density time history from the bottom probe (Probe 1) and the top probe (Probe 2) for  $R/R_{channel} = 1$  at a time of 282 ms corresponding to an axial location of  $Z/R_{channel} = 1.13$ . Cross-correlation between the signals yielded a  $14.4 \mu\text{s}$  delay and the shifted Probe 2 signal in the bottom plot clearly shows how well correlated the signals are. The probe spacing was 26.5 mm yielding a spoke velocity of 1840 m/s in the  $E \times B$  direction. An assumed uncertainty of  $2 \mu\text{s}$  in the delay and 2 mm in the probe position as previously discussed yields a spoke velocity uncertainty of approximately 400 m/s. The discussion in Section 5 regarding the difficulties with uncertainty analysis of Langmuir probe data is rendered moot since the frequencies identified in the PSD (Figure 9) and the delay calculated by vertically spaced probes (Figure 11) do not rely on the magnitude of plasma density oscillations or the mean value.

Figure 12 schematically shows the postulate that spokes represent increased ion production zones. As the spoke rotates, this ion production zone moves azimuthally but the ions produced always move axially once created thereby creating a helical structure within the plume of increased ion density. Note there are always ions being produced in the discharge channel, regardless of spoke location, so there is a constant axial stream of plasma emanating from everywhere in the discharge channel. This possible helical structure would exist in addition to the plume generated globally in the discharge channel. With a spoke velocity of 1800 m/s and an approximate axial ion velocity of 18,000 m/s, the helix angle would be approximately  $6^\circ$ .

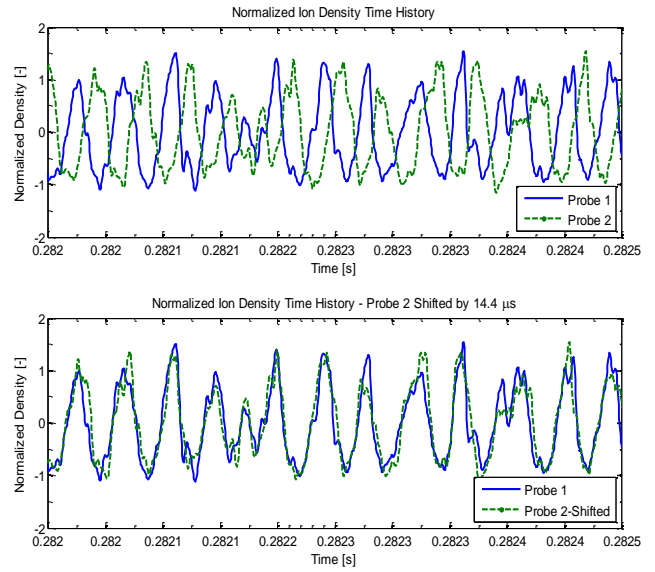


**Figure 11** Probe 1 and 2 both in ion saturation clearly showing coherent plasma oscillations. A  $14.4 \mu\text{s}$  azimuthal signal delay was detected by cross-correlation with a Pearson correlation coefficient of 0.86. The bottom plot shows Probe 2 shifted by  $14.4 \mu\text{s}$  to demonstrate how well correlated the signals were.

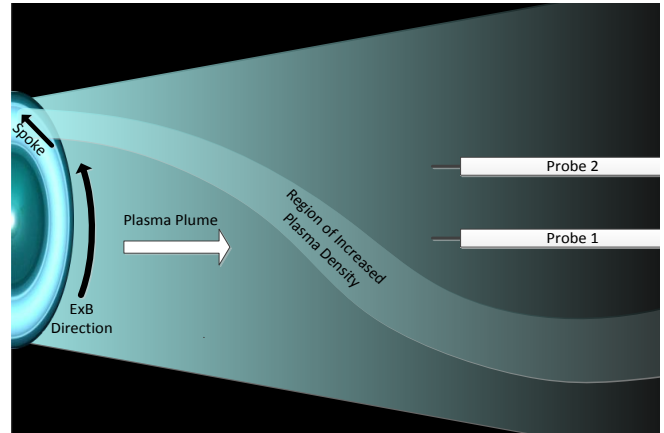


**Figure 12** Illustration of spokes as regions of increased ion density producing helical structures of increased plasma density within the plume and how that would be measured by vertically spaced probes.

## 8. SUMMARY

The methods and tools for high-speed plasma diagnostics including the newly developed HDLP-ISR and the previously discussed FastCam have been described. The time-averaged plasma properties were shown to correlate in general with previous H6 results in similar operating conditions. The time-resolved quantities oscillated about the averaged values demonstrating confidence in the time-resolved plasma properties of  $n_e$ ,  $V_p$  and  $T_e$  from which PSDs and other transient analyses can be performed. The ion and electron density PSD showed interesting peaks at 16, 20, 24 and 28 kHz that did not correlate to the breathing

mode but correlated exactly to azimuthally moving spokes in the thruster observed with high-speed imaging. The time delay from vertically spaced probes suggested a spoke velocity of 1800 m/s which correlates with the results from FastCam analysis. While plasma oscillations due to breathing mode have been observed regularly, the results presented here are the first to positively correlate observed spokes with plasma plume oscillations. The efficiency and stability of HETs is related to the breathing mode and spoke mode oscillations, therefore identification, characterization and understanding of these oscillations including how they originate and interact are an important step to developing end-to-end first principle models of HET operation. Subsequent publications will expand on the results of this testing, investigate the relation between oscillations and electron transport, and finally feed back into the design and integration of HETs into spacecraft systems.

#### ACKNOWLEDGEMENTS

The primary author acknowledges this work was supported by a NASA Office of the Chief Technologist's Space Technology Research Fellowship. The secondary author acknowledges the support of a NASA Strategic University Research Project Grant. A portion of this research was carried out at the Jet Propulsion Laboratory, California Institute of Technology, under a contract with the National Aeronautics and Space Administration and funded through the Director's Research and Development Fund program. The primary author would like to thank Dr. Robert Lobbia for development of and assistance with the HDLP system. The authors would also like to thank Ray Liang, doctoral candidate at PEPL, for the design and construction of the motion stage mounting structure used in this experiment.

#### REFERENCES

- [1] D. Goebel and I. Katz, *Fundamentals of Electric Propulsion: Ion and Hall Thrusters*. Hoboken N.J.: Wiley, 2008.
- [2] E. Y. Choueiri, "Plasma oscillations in Hall thrusters," *Physics of Plasmas*, vol. 8, no. 4, p. 1411, 2001.
- [3] R. Lobbia, M. Sekerak, R. Liang, and A. Gallimore, "High-speed Dual Langmuir Probe Measurements of the Plasma Properties and EEDFs in a HET Plume," paper no. IEPC-2011-168, presented at the 32nd International Electric Propulsion Conference, Wiesbaden, Germany, 2011.
- [4] R. B. Lobbia, "A Time-resolved Investigation of the Hall Thruster Breathing Mode," Ph.D. Dissertation, Dept. of Aerospace Eng., University of Michigan, Ann Arbor, MI, 2010.
- [5] E. Chesta, C. M. Lam, N. B. Meezan, D. P. Schmidt, and M. A. Cappelli, "A characterization of plasma fluctuations within a Hall discharge," *IEEE Transactions on Plasma Science*, vol. 29, no. 4, pp. 582–591, Aug. 2001.
- [6] J. P. Boeuf and L. Garrigues, "Low frequency oscillations in a stationary plasma thruster," *Journal of Applied Physics*, vol. 84, no. 7, p. 3541, 1998.
- [7] J. Fife, M. Martínez-Sánchez, and J. Szabo, "A Numerical Study of Low-Frequency Discharge Oscillations in Hall Thrusters," presented at the 33rd AIAA/ASME/SAE/ASEE Joint Propulsion Conference & Exhibit, Seattle, WA, 1997.
- [8] S. Barral and Z. Peradzyński, "Ionization oscillations in Hall accelerators," *Physics of Plasmas*, vol. 17, no. 1, 2010.
- [9] G. S. Janes and R. S. Lowder, "Anomalous Electron Diffusion and Ion Acceleration in a Low-Density Plasma," *Physics of Fluids*, vol. 9, no. 6, p. 1115, 1966.
- [10] M. McDonald, "Electron Transport in Hall Thrusters," Ph.D. Dissertation, Applied Physics, University of Michigan, Ann Arbor, MI, 2012.
- [11] M. McDonald and A. Gallimore, "Parametric Investigation of the Rotating Spoke Instability in Hall Thrusters," paper no. IEPC-2011-242, presented at the 32nd International Electric Propulsion Conference, Wiesbaden, Germany, 2011.
- [12] M. S. McDonald and A. D. Gallimore, "Rotating Spoke Instabilities in Hall Thrusters," *IEEE Transactions on Plasma Science*, vol. 39, no. 11, pp. 2952–2953, Nov. 2011.
- [13] Y. Raitses, M. Griswold, L. Ellison, J. Parker, and N. Fisch, "Studies of Rotating Spoke Oscillations in Cylindrical Hall Thrusters," paper no. AIAA 2012-4179, presented at the 48th AIAA/ASME/SAE/ASEE Joint Propulsion Conference, Atlanta, GA, 2012.
- [14] C. L. Ellison, Y. Raitses, and N. J. Fisch, "Cross-field electron transport induced by a rotating spoke in a cylindrical Hall thruster," *Physics of Plasmas*, vol. 19, no. 1, 2012.
- [15] D. Brown and A. Gallimore, "Investigation of Low Discharge Current Voltage Hall Thruster Operating Modes and Ionization Processes," paper no. IEPC-2009-074, presented at the 31st International Electric Propulsion Conference, Ann Arbor, MI, 2009.
- [16] R. Hofer, D. Goebel, I. Mikellides, and I. Katz, "Design of a Laboratory Hall Thruster with Magnetically Shielded Channel Walls, Phase II: Experiments," paper no. AIAA 2012-3789, presented at the 48th AIAA/ASME/SAE/ASEE Joint Propulsion Conference & Exhibit, Atlanta, GA, 2012.
- [17] B. M. Reid, "The Influence of Neutral Flow Rate in the Operation of Hall Thrusters," Ph.D. Dissertation, Dept. of Aerospace Eng., University of Michigan, Ann Arbor, MI, 2009.
- [18] K. K. Jameson, "Investigation of hollow cathode effects on total thruster efficiency in a 6 kW Hall thruster," Ph.D. Dissertation, Dept. of Aerospace Eng., University of California, Los Angeles, Los Angeles, CA, 2008.
- [19] D. L. Brown, "Investigation of Low Discharge Voltage Hall Thruster Characteristics and Evaluation of Loss Mechanisms," Ph.D. Dissertation, Dept. of Aerospace Eng., University of Michigan, Ann Arbor, MI, 2009.

- [20] R. Shastry, "Experimental Characterization of the Near-Wall Region in Hall Thrusters and its Implications on Performance and Lifetime," Ph.D. Dissertation, Dept. of Aerospace Eng., University of Michigan, Ann Arbor, MI, 2011.
- [21] W. Huang, "Study of Hall Thruster Discharge Channel Wall Erosion via Optical Diagnostics," Ph.D. Dissertation, Dept. of Aerospace Eng., University of Michigan, Ann Arbor, MI, 2011.
- [22] R. Hofer, I. Mikellides, I. Katz, and D. Goebel, "Wall Sheath and Electron Mobility Modeling in Hybrid-PIC Hall Thruster Simulations," paper no. AIAA 2007-5267, presented at the 43rd AIAA/ASME/SAE/ASEE Joint Propulsion Conference & Exhibit, Cincinnati, OH, 2007.
- [23] I. Mikellides, I. Katz, R. Hofer, and D. Goebel, "Hall-Effect Thruster Simulations with 2-D Electron Transport and Hydrodynamics Ions," paper no. IEPC-2009-114, presented at the 31st International Electric Propulsion Conference, Ann Arbor, MI, 2009.
- [24] M. McDonald, C. Bellant, B. St Pierre, and A. Gallimore, "Measurement of Cross-Field Electron Current in a Hall Thruster Due to Rotating Spoke Instabilities," paper no. AIAA 2011-5810, presented at the 47th AIAA/ASME/SAE/ASEE Joint Propulsion Conference & Exhibit, San Diego, CA, 2011.
- [25] F. F. Chen, "Electric Probes," in *Plasma Diagnostic Techniques*, R. H. Huddlestone, Ed. New York: Academic Press, 1965, pp. 113–200.
- [26] B. E. Cherrington, "The use of electrostatic probes for plasma diagnostics - A review," *Plasma Chemistry and Plasma Processing*, vol. 2, no. 2, pp. 113–140, Jun. 1982.
- [27] N. Hershkowitz, "How Langmuir Probes Work," in *Plasma diagnostics.*, vol. 1. Discharge parameters and chemistry, 2 vols., O. Auciello and D. L. Flamm, Eds. Boston: Academic Press, 1989, pp. 113–183.
- [28] R. H. Huddlestone, Ed., *Plasma diagnostic techniques*. New York: Academic Press, 1965.
- [29] I. H. Hutchinson and Cambridge University Press, *Principles of Plasma Diagnostics*. Cambridge: Cambridge University Press, 2002.
- [30] L. Schott, "Electrical Probes," in *Plasma Diagnostics*, W. Lochte-Holtgreven, Ed. Amsterdam: North-Holland Publishing Company, 1968, pp. 668–731.
- [31] J. D. Swift and M. J. R. Schwar, *Electrical probes for plasma diagnostics*. London; New York: Iliffe Books; American Elsevier, 1969.
- [32] M. A. Lieberman and A. J. Lichtenberg, *Principles of plasma discharges and materials processing*. Hoboken, N.J.: Wiley-Interscience, 2005.
- [33] R. B. Lobbia and A. D. Gallimore, "High-speed dual Langmuir probe," *Review of Scientific Instruments*, vol. 81, no. 7, p. 073503, 2010.
- [34] R. B. Lobbia and A. D. Gallimore, "Temporal limits of a rapidly swept Langmuir probe," *Physics of Plasmas*, vol. 17, no. 7, p. 073502, 2010.
- [35] R. B. Lobbia, "A Time-resolved Investigation of the Hall Thruster Breathing Mode," Ph.D. Dissertation, University of Michigan, Ann Arbor, MI, 2010.
- [36] F. W. Crawford and R. Gard, "Low-Frequency Impedance Characteristics of a Langmuir Probe in a Plasma," *Journal of Applied Physics*, vol. 37, no. 1, p. 180, 1966.
- [37] R. R. Hofer, "Development and characterization of high-efficiency, high-specific impulse xenon Hall thrusters.," Ph.D. Dissertation, Dept. of Aerospace Eng., 2004.
- [38] K. A. Graf, "Comparison of Langmuir Probe and Microwave Diagnostic Techniques," *Journal of Applied Physics*, vol. 38, no. 11, p. 4466, 1967.

## BIOGRAPHIES



**Michael Sekerak** received a B.S. in Mechanical Engineering from Illinois Institute of Technology in 1999 and an M.S. in Aeronautics and an Engineer's Degree from California Institute of Technology in 2001 and 2005, respectively, while conducting research at NASA JPL. He served in the Army as a cavalry officer including one combat tour in Iraq and the Missile Warning Center in Cheyenne Mountain. He is a Major in the Air Force Reserves teaching with the Reserve National Security Space Institute. Prior to the Ph.D. program at University of Michigan, he was an aerospace engineer with the Missile Systems group at Sandia National Laboratories.



**Michael McDonald** received B.S.E. degrees in Aerospace Engineering and Engineering Physics and the Ph.D. degree in Applied Physics from the University of Michigan, Ann Arbor, MI in 2006 and 2011, respectively. He was previously a National Science Foundation Graduate Research Fellow and is currently a post-doctoral research scientist at the University of Michigan Plasmadynamics and Electric Propulsion Laboratory, conducting investigations into cross-field electron transport mechanisms in the Hall thruster plasma. His research interests include high-speed plasma diagnostics, digital signal processing including image processing, low-temperature plasma physics and plasma instabilities, and electric spacecraft propulsion.



**Richard Hofer** received the B.S.E. degree in mechanical engineering and the B.S.E., M.S.E, and Ph.D. degrees in aerospace engineering from the University of Michigan, Ann Arbor, MI, in 1998, 1998, 2000, and 2004, respectively. He is a Senior Engineer at the Jet Propulsion Laboratory where he is the technology lead responsible for the development and

*qualification of Hall thrusters for deep space missions. He is a recognized expert in Hall thruster design, having designed several advanced Hall thrusters ranging in power from 1 to 100 kW. Thruster technology developed by Dr. Hofer is now used in every internal Hall thruster development of the United States Government. In 2011, he received the NASA Exceptional Achievement Medal and the JPL Lew Allen Award for Excellence. Dr. Hofer is an Associate Fellow of the AIAA and a member of the AIAA Electric Propulsion Technical Committee. He has authored over 65 technical publications in the field of electric propulsion.*



***Alec Gallimore** is an Arthur F. Thurnau Professor of Aerospace Engineering at the University of Michigan where he directs the Plasmadynamics and Electric Propulsion Laboratory. He received his B.S. in Aeronautical Engineering from Rensselaer, and his M.A. and*

*Ph.D. degrees in Aerospace Engineering with an emphasis in plasma physics from Princeton. His primary research interests include electric propulsion, plasma diagnostics, use of plasma for environmental remediation, and nano-particle physics. He is the author of 300 journal and conference papers on electric propulsion and plasma physics, and is a Fellow of the American Institute of Aeronautics and Astronautics (AIAA).*

## APPENDIX A

### Example I-V Analysis

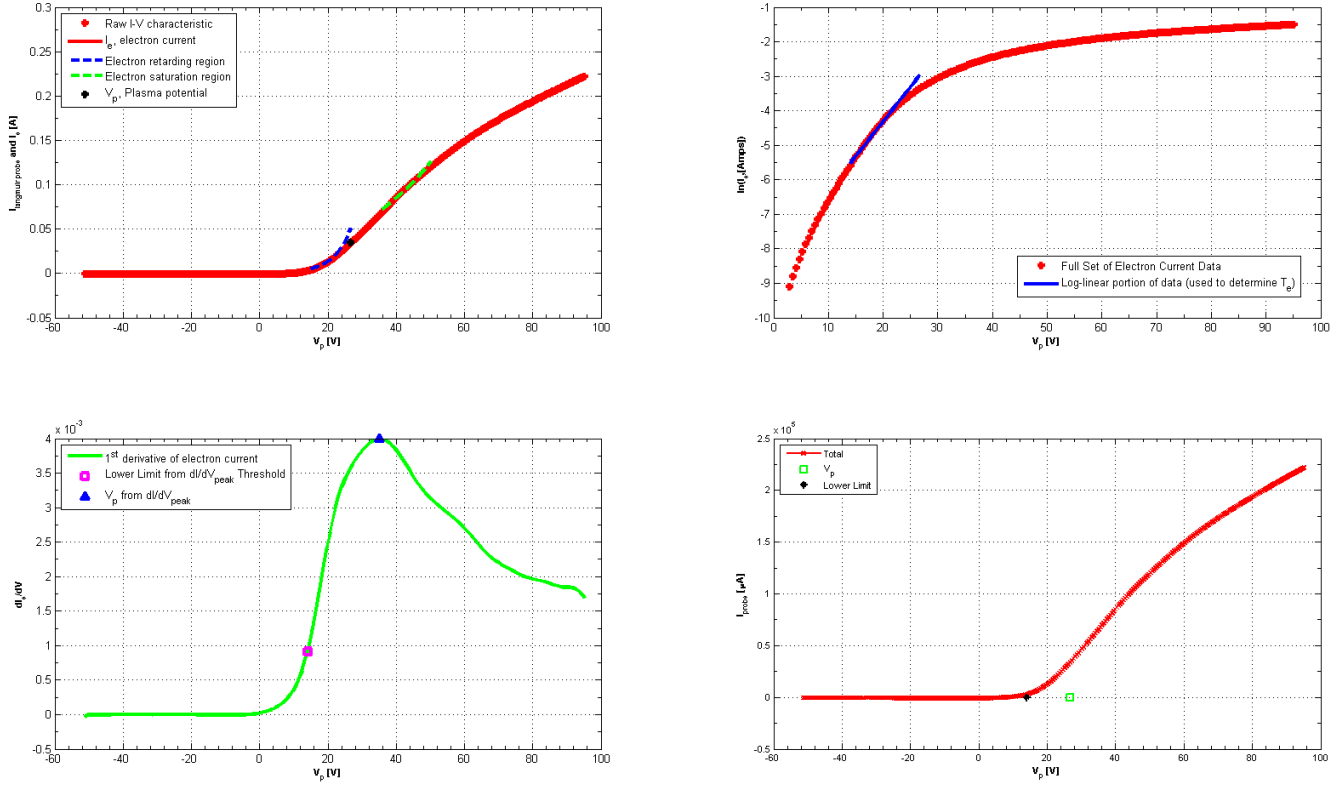


Figure 13 Example I-V analysis at  $R/R_{channel} = Z/R_{channel} = 1$  showing the I-V trace, the natural log of electron current and the linear fit for  $T_e$  calculation, and  $dI_e/d\phi$  with the peak identified for  $V_p$  and  $I_{e, sat}$ .

APPENDIX B

Time Averaged Plasma Property Contour Maps

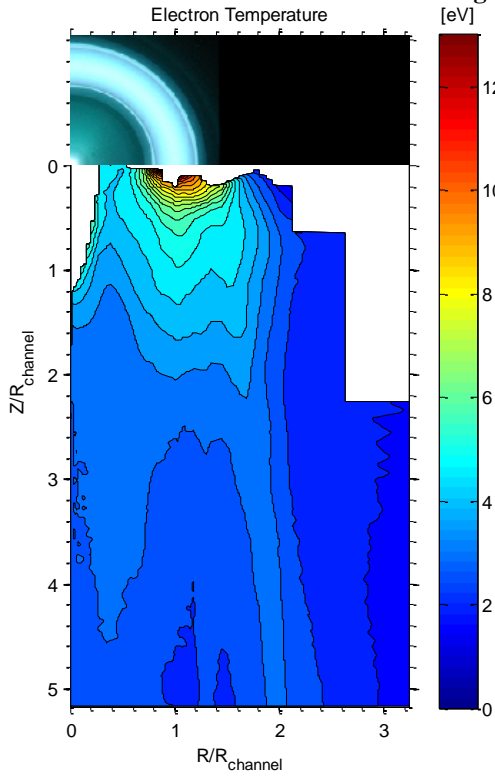


Figure 14 Time averaged electron temperature. Contour interval is 0.5 eV.

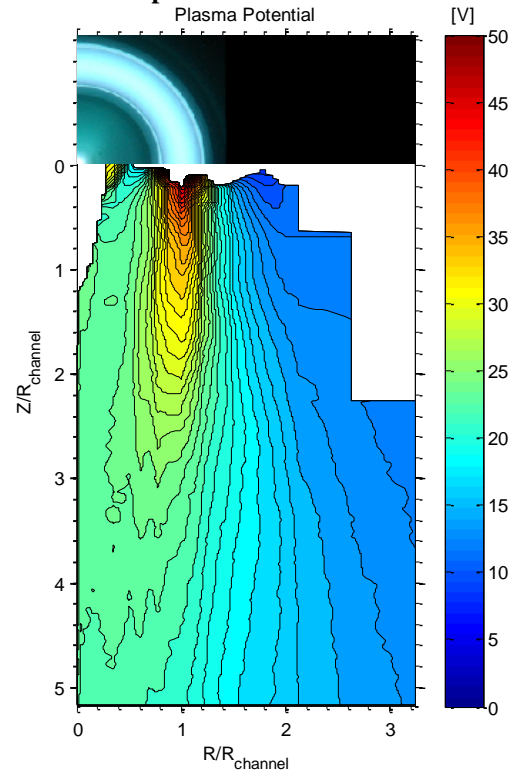


Figure 15 Time averaged plasma potential. Contour interval is 1.0 V.

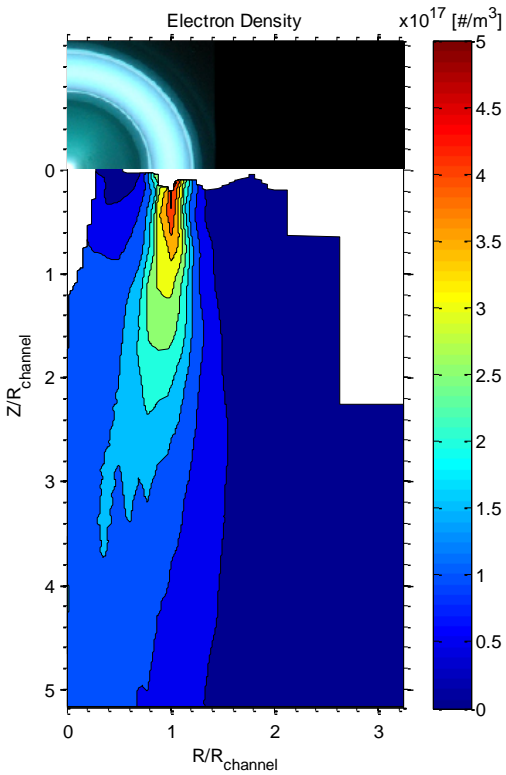


Figure 16 Time averaged electron density. Contour interval is  $1 \times 10^{-16}$  #/m<sup>3</sup>.